Article

Developmental Cell

A Conserved Phosphorylation Switch Controls the Interaction between Cadherin and β-Catenin In Vitro and In Vivo

Highlights

- Conserved phospho-Ser1212 in *C. elegans* cadherin is required for binding to β-catenin
- Loss of HMR-1 Ser1212 phosphorylation produces severe adhesion defects
- Sequence differences in β-catenin homologs define roles in adhesion and Wnt signaling

Authors

Hee-Jung Choi, Timothy Loveless, ..., Jeff Hardin, William I. Weis

Correspondence

choihj@snu.ac.kr (H.-J.C.), bill.weis@stanford.edu (W.I.W.)

In Brief

Choi et al. identify a phosphoserine in the tail of the *C. elegans* cadherin HMR-1 required for strong binding to the β-catenin homolog HMP-2 during cell adhesion. Structural analysis allows the authors to define sequence differences among worm β-catenin homologs that explain their separate roles in adhesion and Wnt signaling.

Accession Numbers

4R0Z
4R10
4R11

Choi et al., 2015, Developmental Cell *33*, 82–93
April 6, 2015
http://dx.doi.org/10.1016/j.devcel.2015.02.005

CellPress

CellPress

Developmental Cell
Article

A Conserved Phosphorylation Switch Controls the Interaction between Cadherin and β-Catenin In Vitro and In Vivo

Hee-Jung Choi,[1,5,*] Timothy Loveless,[2,5] Allison M. Lynch,[3] Injin Bang,[1] Jeff Hardin,[2,3,6] and William I. Weis[4,6,*]
[1]School of Biological Sciences, Seoul National University, Seoul 151-747, South Korea
[2]Program in Cellular and Molecular Biology, University of Wisconsin, Madison, WI 53706, USA
[3]Department of Zoology, University of Wisconsin, Madison, WI 53706, USA
[4]Departments of Structural Biology and of Molecular and Cellular Physiology, Stanford University School of Medicine, Stanford, CA 94305, USA
[5]Co-first author
[6]Co-senior author
*Correspondence: choihj@snu.ac.kr (H.-J.C.), bill.weis@stanford.edu (W.I.W.)
http://dx.doi.org/10.1016/j.devcel.2015.02.005

SUMMARY

In metazoan adherens junctions, β-catenin links the cytoplasmic tail of classical cadherins to the F-actin-binding protein α-catenin. Phosphorylation of a Ser/Thr-rich region in the cadherin tail dramatically enhances affinity for β-catenin and promotes cell-cell adhesion in cell culture systems, but its importance has not been demonstrated in vivo. Here, we identify a critical phosphorylated serine in the *C. elegans* cadherin HMR-1 required for strong binding to the β-catenin homolog HMP-2. Ablation of this phosphoserine interaction produces developmental defects that resemble full loss-of-function (Hammerhead and Humpback) phenotypes. Most metazoans possess a single gene for β-catenin, which is also a transcriptional coactivator in Wnt signaling. Nematodes and planaria, however, have a set of paralogous β-catenins; for example, *C. elegans* HMP-2 functions only in cell-cell adhesion, whereas SYS-1 mediates transcriptional activation through interactions with POP-1/Tcf. Our structural data define critical sequence differences responsible for the unique ligand specificities of these two proteins.

INTRODUCTION

Cell-cell adhesion is fundamental to the generation and structure of multicellular tissues. The classical cadherin cell adhesion molecules mediate homophilic adhesion and are linked to the actin cytoskeleton through the catenins (Pokutta and Weis, 2007). β-Catenin binds to the cytoplasmic tail of classical cadherins, and to α-catenin, an F-actin binding protein. β-Catenin is a highly conserved metazoan protein that functions in cell-cell adhesion and as a transcriptional coactivator in the Wnt/β-catenin pathway. β-Catenin has an N-terminal region of roughly 150 amino acids, followed by 12 armadillo (arm) repeats, each comprised of three α helices, and a C-terminal acidic tail that mediates interactions with components of the general transcription apparatus. Structural studies have shown that the different partners of β-catenin involved in adhesion (the classical cadherin cytoplasmic domain) and in Wnt signaling (TCF transcription factors, ICAT, the Adenomatous Polyposis Coli protein, and Axin) interact similarly with the arm domain (Pokutta and Weis, 2007).

In most metazoans, a single gene encodes a β-catenin that functions in both cadherin-based adhesion and transcriptional coactivation via Wnt signaling. An exception is *C. elegans*, a nematode that expresses four distinct β-catenin paralogs, only one of which, HMP-2, functions in cell adhesion. It is therefore of interest to understand how these different paralogs have evolved to mediate distinct functions by binding to partners involved in adhesion versus signaling. *C. elegans* also expresses the cadherin HMR-1, whose cytoplasmic domain bears significant sequence homology to that of mammalian classical cadherins, and the α-catenin homolog HMP-1 (Costa et al., 1998; Cox and Hardin, 2004).

Studies in cell culture have revealed that interactions among adherens junction (AJ) components can be regulated by phosphorylation. A serine-rich region of the classical cadherin tail is phosphorylated (Stappert and Kemler, 1994), and in vitro phosphorylation of the purified cadherin tail by glycogen synthase kinase 3β (GSK-3β) and casein kinase II (CKII) strengthens its affinity for β-catenin ~800-fold by creating an additional interaction surface (Choi et al., 2006; Huber and Weis, 2001; Lickert et al., 2000). Mutation of the phosphorylated serines to alanine reduced cell-cell adhesion when these constructs were transfected into NIH 3T3 cells (Lickert et al., 2000). Gottardi and colleagues recently narrowed these phosphorylation sites to three residues that are required for high-affinity β-catenin binding, cell adhesion, inhibition of cell migration, and surface stability of cadherin in cultured cells (McEwen et al., 2014). In contrast, Src-mediated phosphorylation of β-catenin Tyr654 reduces affinity for cadherin (Roura et al., 1999), and CKII phosphorylation of β-catenin regulates its interaction with α-catenin (Bek and Kemler, 2002).

Although there are strong correlations between dysregulation of AJ assembly and disease such as metastatic cancers (Benjamin and Nelson, 2008; van Roy, 2014), the functional

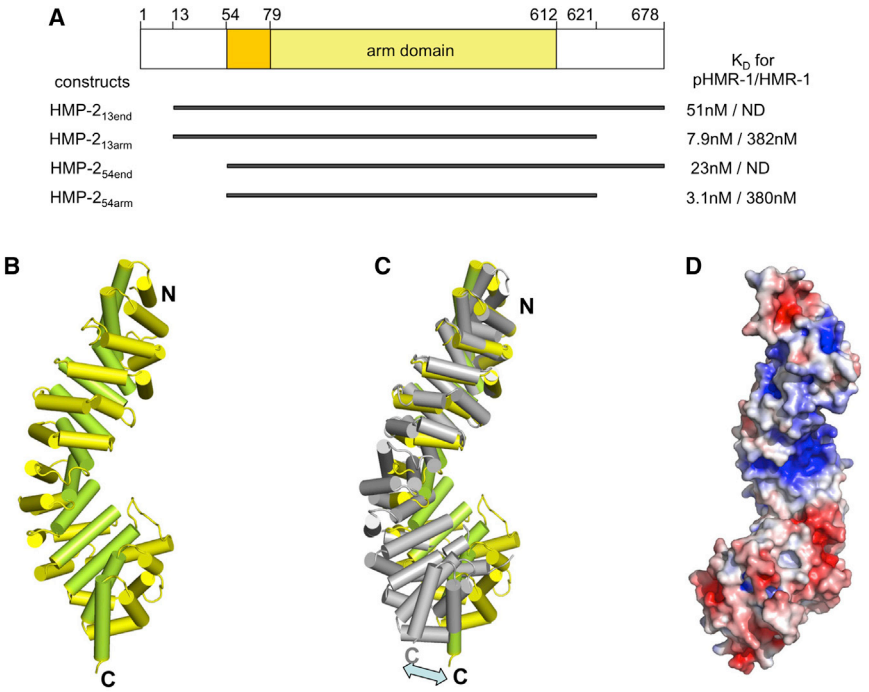

Figure 1. HMP-2 Structure and Dependence of Binding on the Phosphorylation State of HMR-1

(A) Four constructs of HMP-2, which were used in our study, are shown and their residue boundaries indicated. On the right side of each construct, K_D values for pHMR-1_{cyto80} and HMR-1_{cyto80}, measured by ITC experiments, are shown. HMP-2_{13end} and HMP-2_{54end} did not give measurable ITC signals for the interaction with HMR-1_{cyto80} and are labeled as ND.

(B) Structure of HMP-2_{54arm} (residues 77–613). Helices 1 and 2 of each arm repeat are colored yellow, and helix 3 is colored light green. The structures of HMP-2_{54arm} and HMP-2_{54end} are very similar except for the N-terminal region. Residues 56–79 are seen only in the HMP-2_{54end} structure, and they form an extra N-terminal helix whose position appears to be a consequence of crystal packing.

(C) Superposition of arm repeats 1–4 of HMP-2 and mouse β-catenin (PDB ID: 1I7W). HMP-2 helices are colored as in (B) and β-catenin is colored gray.

(D) Electrostatic surface of the HMP-2 arm domain, with negative and positive regions colored red and blue, respectively. Contoured at ±5 k_BT/e.

effects of phosphorylation of AJ components have not been examined in a true in vivo setting. *C. elegans* offers a system with which to test effects of phosphorylative regulation in vivo. Here, we use biochemical and structural methods to identify a critical phosphorylated serine in the tail of the *C. elegans* cadherin HMR-1 required for binding to the β-catenin homolog HMP-2. Mutation of this serine, or a set of arginine residues in HMP-2 that coordinate the phosphate group, produces severe developmental defects, demonstrating the physiological importance of a posttranslational modification identified from biochemical and structural approaches. Likewise, a phosphomimetic mutation of a conserved tyrosine in β-catenin/HMP-2 produces significant developmental phenotypes that correlate with the effect of phosphorylation of this residue in higher organisms. The structural data also allow us to define critical sequence differences responsible for the unique ligand specificities of HMP-2 and SYS-1.

RESULTS

Similarities between HMP-2 and β-Catenin

HMP-2 is homologous to mammalian β-catenin, with a central 12 arm repeat domain (33% identity and 52% similarity to the mouse β-catenin arm domain) flanked by N- and C-terminal tails that are shorter than those of mammalian β-catenin (Figures 1A and S1). In particular, HMP-2 lacks the N-terminal phosphorylation-dependent degron present in mammalian β-catenins that is critical for regulation of β-catenin in Wnt signaling (Stamos and Weis, 2013). Nonetheless, the N-terminal region contains sequences homologous to the α-catenin binding site of β-catenin that mediate similar interactions with α-catenin (Kwiatkowski et al., 2010). The C-terminal tail of mammalian β-catenins is the interaction site for general transcription factors needed for β-catenin function as a transcriptional coactivator (Barker et al., 2001; Hecht et al., 1999, 2000; Miyagishi et al., 2000; Takemaru and Moon, 2000; Tutter et al., 2001); the HMP-2 tail is shorter and is not homologous in this region.

We determined the structure of an HMP-2 construct consisting of residues 54–678, designated HMP-2_{54end}, which comprises a portion of the HMP-1/α-catenin binding site, the arm domain, and C-terminal region (Figure 1A), at 2.0-Å resolution (Table S1; Figure 1B). The visible structure contains the 12 predicted arm repeats, and an extra helix (residues 54–71) at the N terminus preceding the arm repeats, which corresponds to the α-catenin binding helix formed by mouse β-catenin 121–149. This helix is engaged in lattice packing interactions, so it is unclear whether its position is functionally relevant.

Although the C-terminal tail (residues 613–678) is part of the crystallized construct, it was not visible in the structure; in particular, the extra α helix ("helix C") found just after the arm repeats in crystals of full-length zebrafish β-catenin (Xing et al., 2008) and in plakoglobin (Choi et al., 2009) is absent. The sequence of helix C is conserved in human, mouse, zebrafish, and *Drosophila* β-catenins, whereas the corresponding portion of the HMP-2 sequence lacks these residues and is predicted to have no secondary structure. Helix C contributes to the interaction with the Wnt transcription antagonists ICAT and Chibby (Xing et al., 2008). The absence of helix C in HMP-2 is consistent with its specialized function as a cell adhesion protein.

Superposition of the arm domains of HMP-2 and β-catenin shows that although the individual arm repeats are similar, the curvatures of the superhelix are different; the C-terminal halves of the domain are displaced by ~20 Å when the N-terminal halves are aligned, and vice versa (Figure 1C). The arm domains of HMP-2, β-catenin, p120, plakoglobin, plakophilin, and SYS-1 have different curvatures, likely due to small differences in the

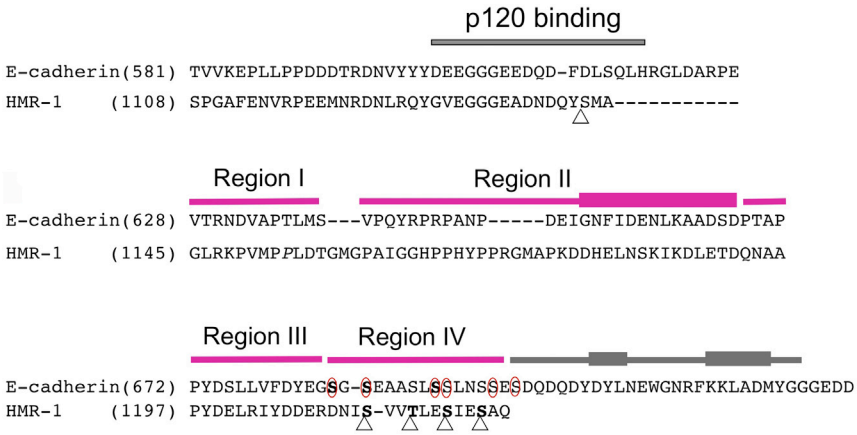

Figure 2. Sequence Alignment of the Cytoplasmic Tails of Mouse E-Cadherin and HMR-1 Reveals Key Conserved Residues

The juxtamembrane region including the p120 (JAC-1 in *C. elegans*) binding site was aligned based on sequence homology, and the β-catenin (HMP-2) binding region was aligned based on the crystal structures of pE_{cyto} and $pHMR\text{-}1_{cyto80}$. The HMP-2 binding domain is divided into four regions, and each region is indicated with magenta bar on top of the sequences. The C-terminal cap region is only present in E_{cyto} and is shown as a gray-colored bar. The thickened rectangles represent α helices. Five CKI-phosphorylated sites in $HMR\text{-}1_{cyto}$ are marked with triangles, and six sites phosphorylated by GSK-3β and CKII in E_{cyto} are circled. Phosphorylated residues observed in the structures are written in bold (three residues in pE_{cyto} and four in $pHMR_{cyto80}$). The starting residue numbers are indicated.

packing of arm repeats. However, all of these proteins feature a positively charged groove formed by the superhelix, and their overall isoelectric points (pIs) are ~8 or above. In β-catenin, this groove is the common binding site for many different ligands, including cadherins, TCFs, Adenomatous Polyposis Coli protein (APC), and ICAT (Pokutta and Weis, 2007). Curiously, the overall pI of the arm domain of HMP-2 is ~5.5, but it contains a positively charged groove similar to these other arm domain structures (Figure 1D).

HMR-1 Must Be Phosphorylated in Order to Bind Strongly to HMP-2

The cytoplasmic domains of HMR-1 and murine E-cadherin bear significant sequence homology (25% identity, 34% similarity) (Figure 2). The crystal structure of the 151-amino-acid E-cadherin cytoplasmic domain (E_{cyto}) bound to the β-catenin arm domain revealed that the last 100 amino acids of E_{cyto} constitute the β-catenin binding site. E_{cyto} features five regions of interaction with β-catenin (Huber and Weis, 2001). Region I, the N-terminal portion of the binding site, packs against arm repeats 8 and 9 and also interacts with region III. Region II includes an amphipathic α helix that forms a hydrophobic interface with β-catenin arm repeats 11 and 12. Region III is an extended peptide that binds in the groove formed by arm repeats 5–10, and includes the $Dx\theta\theta x\phi x_{2-7}E$ (θ represents non-polar aliphatic interaction, ϕ represents aromatic) motif that defines the interactions of β-catenin with Wnt pathway ligands, including TCFs, APC, and ICAT (Pokutta and Weis, 2007). Region IV is a serine-rich motif that binds to β-catenin only when phosphorylated, a modification that increases the affinity of E_{cyto} for β-catenin from 46 nM to 52 pM. The C-terminal region V, also called the hydrophobic cap, contains two short α helices that pack against what would otherwise be exposed hydrophobic residues at the start of the arm domain. Sequence alignment (Figure 2) indicates that the amphipathic helix in region II and the region III $Dx\theta\theta x\phi x_{2-7}E$ motif are present in HMR-1, and a serine-rich sequence is present in region IV. However, HMR-1 is truncated relative to E-cadherin and lacks the region V cap.

Despite the similarities between the *C. elegans* and mammalian proteins, there was no detectable interaction between bacterially expressed HMR-1 cytoplasmic domain ($HMR\text{-}1_{cyto}$) and $HMP\text{-}2_{54end}$, as assessed by isothermal titration calorimetry (ITC) (Figures 1A and S2; Table S2) and co-migration on a gel filtration column (Kwiatkowski et al., 2010). This is consistent with the absence of the region V cap in HMR-1, as deletion of this region significantly weakens the interaction of E-cadherin with β-catenin (Finnemann et al., 1997; Stappert and Kemler, 1994). Curiously, HMP-2 lacking the C-terminal tail ($HMP\text{-}2_{54arm}$) bound weakly, but detectably, to $HMR\text{-}1_{cyto}$ (K_D = 380 nM) in ITC (Figures 1A and S2; Table S2). This behavior is reminiscent of mammalian β-catenin binding to its weaker ligands Axin and APC, where deletion of its C-terminal tail increases the affinity for Axin and APC-R3 by 7-fold and 15-fold, respectively (Choi et al., 2006). However, the C-terminal tail does not affect binding of β-catenin to tightly binding ligands including E-cadherin and LEF-1 (Choi et al., 2006). We also tested the effect of the N-terminal tail of HMP-2. Full-length HMP-2 could not be expressed as a soluble protein in *E. coli*, so constructs in which the N-terminal 12 amino acids were deleted ($HMP\text{-}2_{13end}$ and $HMP\text{-}2_{13arm}$; Figures 1A and S2) were used for these experiments. The data showed that residues 13–53 of HMP-2 had no significant effect on the affinity for HMR-1 (Table S2). This is consistent with ITC data of β-catenin indicating that the N-terminal domain has no or very minor effect on ligand binding (Choi et al., 2006).

Phosphorylation of E_{cyto} by GSK-3β and CKII increases the affinity for β-catenin ~800-fold, due to the interaction of the phosphorylated region IV with arm repeats 3–5 (Choi et al., 2006; Huber and Weis, 2001). The HMR-1 cytoplasmic domain contains four consensus casein kinase I (CKI) sites in region IV, as well as a fifth CKI site in the juxtamembrane region (Figure 2). Specifically, CKI prefers substrates with an acidic side chain or a phosphorylated Ser/Thr three residues N-terminal to the target phosphorylation site: in region IV, Ser1212 is preceded by Asp1209 and is followed by Thr1215, Ser1218, and Ser1221 (Figure 2). Anion exchange chromatography following in vitro phosphorylation of $HMR\text{-}1_{cyto}$ with CKI gave two peaks, both of which eluted at a higher salt concentration relative to non-phosphorylated $HMR\text{-}1_{cyto}$ (data not shown). Mass spectrometric analysis confirmed that the two peaks have four and

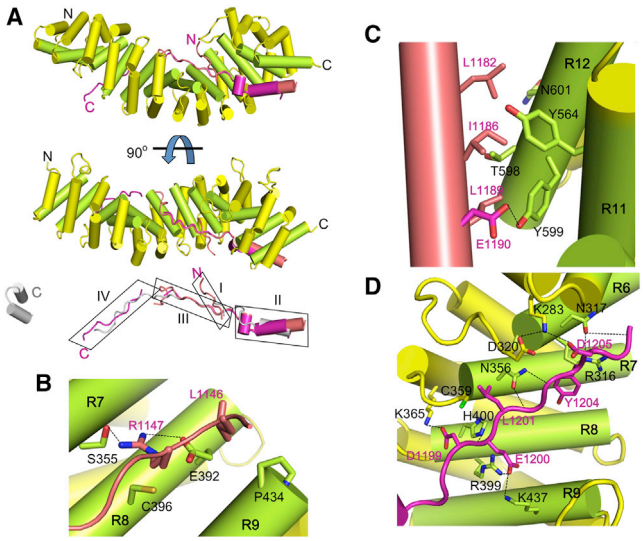

Figure 3. Crystal Structure of HMP-2_{54arm}/pHMR-1_{cyto80} Complex Identifies Key Interaction Regions

In each panel, the arm domain is colored as in Figure 1B, and the structures of pHMR-1_{cyto80} are shown in salmon (conformation A from the high-resolution $P4_3$ crystal form) and magenta (conformation B).

(A) Ribbon diagram of the complex. The N terminus and C terminus of each protein are labeled. In the lower panel, phosphorylated E_{cyto} is aligned to pHMR-1_{cyto80} (shown in gray). The four regions of pHMR-1 are boxed and labeled as I, II, III, and IV.

(B) Interaction region I. Arm repeats 7, 8, and 9 are labeled as R7, R8, and R9, respectively. Side chains of amino acids that make direct contacts between HMP-2 and pHMR-1_{cyto} are shown as sticks, and HMP-2 and pHMR-1 residues are labeled in black and magenta, respectively. Hydrogen bonds are shown as dotted lines.

(C) Interaction region II.

(D) Interaction region III. Most of the contacts between HMP-2 and pHMR-1_{cyto} are formed by side chains, except for N317, N356, and H400 of HMP-2, which form hydrogen bonds with amide and carbonyl groups of the pHMR-1_{cyto} backbone.

five phosphorylated residues, respectively. It is likely that the four serines in region IV are sequentially phosphorylated by CKI, with the fifth site the juxtamembrane Ser1142.

CKI-mediated phosphorylation of purified HMR-1_{cyto} produced a dramatic increase in affinity for HMP-2: both phosphorylated HMR-1_{cyto} (pHMR-1_{cyto}) fractions, with either four or five phosphorylated residues, were found to co-elute with HMP-2 on a size exclusion column (Kwiatkowski et al., 2010). The β-catenin binding region of E-cadherin is homologous to the last 80 amino acids of HMR-1 (Figure 2), so a construct corresponding to this region, designated HMR-1_{cyto80}, was tested for HMP-2 binding by ITC. The 380 nM dissociation constant of HMP-2_{54arm} for HMR-1_{cyto80} was decreased to 3.1 nM for pHMR-1_{cyto80} (Figures 1A and S2; Table S2). To test whether the tails of HMP-2 affect the affinity for pHMR-1_{cyto80}, ITC experiments were performed using HMP-2_{13end} and HMP-2_{54end}. The presence of the C-terminal tail of HMP-2 weakens the affinity ~7-fold (23 nM versus 3.1 nM), whereas the presence of the N-terminal tail did not significantly affect binding to pHMR-1 (Figures 1A and S2; Table S2).

The increase in affinity for HMP-2 associated with phosphorylation of HMR-1 parallels the change in murine E-cadherin affinity for β-catenin; in both cases, phosphorylation increases affinity more than two orders of magnitude. However, the absolute affinities differ dramatically: without phosphorylation, E-cadherin binds to β-catenin with an affinity of 46 nM, whereas comparable affinity is achieved for HMR-1 only when it is phosphorylated.

Crystal Structure of pHMR-1 Bound to HMP-2

To define the mechanism of phosphorylation-dependent binding of HMR-1 to HMP-2, we obtained crystal structures of the pHMR-1/HMP-2 complex. The complex of individually purified HMP-2_{54arm} and in vitro CKI-pHMR-1_{cyto80} (pHMR-1_{cyto80}) was prepared by gel filtration chromatography and crystallized in two different conditions (Table S1). The two structures were determined at 2.3- and 2.8-Å resolution and provided four independent views of the complex, one in the higher-resolution $P4_3$ crystal form and three in the $P2_1$ form (Figure 3A). The four copies of HMR-1_{cyto80} align well in regions II and III, whereas region I is visible only in three copies. The phosphorylated region IV adopts two different conformations; three copies (the single $P4_3$ and two of the $P2_1$ copies) adopt the same conformation, designated conformation A, whereas the other is distinct (conformation B).

Apart from the absence of region V, the overall binding mode of HMR-1_{cyto80} for HMP-2 is very similar to that of E-cadherin binding to β-catenin (Figure 3A). Region I interacts with side chains from arm repeats 7, 8, and 9 (Figure 3B). Residues 1153–1178, which connect regions I and II, are disordered. Hydrophobic residues on the amphipathic helix in region II pack against HMP-2 residues located on arm repeats 11 and 12, including Tyr599 (see below) (Figure 3C). The polypeptide then makes a sharp turn into region III, which adopts an extended conformation that interacts with the basic groove of the arm domain in essentially the same way as observed between murine E-cadherin and β-catenin (Figure 3D). The polypeptide backbone of region III forms hydrogen bonds with polar residues on arm repeats 6, 7, and 8 of HMP-2. Asp1199, the first residue of the $Dx\theta\theta x\phi x_{2-7}E$ motif, forms a salt bridge with HMP-2 Lys365. Leu1201 packs against Cys359, and Tyr1204 packs against HMP-2 Arg316. In two of the four independent copies of the complex, Glu1207, the last residue of the consensus region III motif, forms a salt bridge with Lys240 of HMP-2. In addition to the interactions in common with the E-cadherin/β-catenin complex, Glu1200 of HMR-1 forms salt bridges with Arg399 and Lys437 of HMP-2.

The mass spectrometry analysis of in vitro pHMR-1 suggested that four residues in region IV are sequentially phosphorylated by CKI. In pHMR-1 conformation A, only the first phosphorylated residue, Ser1212, is observed; all of the HMR-1 residues C-terminal to this position are disordered (Figures 4A and 4B). In conformation B, region IV is disconnected from region III by three missing residues, 1208–1210, but it continues until A1222, the penultimate HMR-1 residue. Notably, all four phosphorylated residues (S1212, T1215, S1218, S1221) are visible (Figure 4A) in conformation B, which superimposes closely with that of phosphorylated E-cadherin bound to β-catenin (Figures 4C and 4D). In contrast, conformation A appears to arise from displacement by neighboring molecules in the crystal. We conclude that conformation B represents the solution conformation of the bound pHMR-1.

In conformation B, the side chains of V1214, L1216, and I1219 pack against residues from HMP-2 arm repeats 4 and 5,

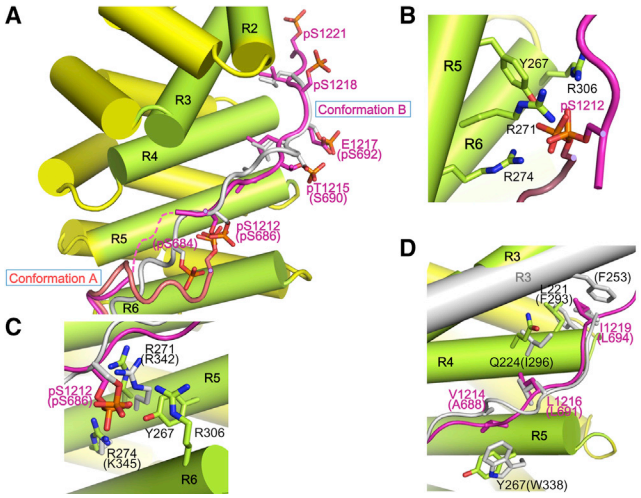

Figure 4. Phosphorylation Generates Specific Interactions of HMR-1 Region IV with HMP-2

(A) Structures of HMP-2 bound to the two different conformations of pHMR-1_{cyto} are aligned, with conformations A and B shown in salmon and magenta, respectively. Also shown is a superposition of pE_{cyto} (gray) from the β-$catenin_{arm}$/pE_{cyto} complex structure (PDB ID: 1I7W) with conformation B of pHMR-1_{cyto}; E-cadherin residues are indicated in parentheses. For clarity, the superimposed arm domain β-catenin is not shown. All phosphorylated residues observed in the structures of pE_{cyto} and pHMR-1_{cyto} are represented.

(B) Close-up of the interactions between HMP-2 and pS1212 of pHMR-1_{cyto} from conformations A and B.

(C) Comparison of HMR-1 pS1212 interactions with HMP-2 and E-cadherin pS686 with β-catenin.

(D) Comparison of β-catenin-pE_{cyto} interactions with those of HMP-2–pHMR-1_{cyto} residues 1214–1219.

analogous to the hydrophobic interactions mediated by phosphorylated E-cadherin A688, L691, and L694 with β-catenin (Figure 4D). Moreover, HMR-1 pT1215 forms a salt bridge with HMP-2 K264; the equivalent residue in E-cadherin, S690, is not phosphorylated and points away from the surface of β-catenin. Given the disorder of region IV in the non-phosphorylated mammalian E-cadherin/β-catenin complex, we expect that region IV of non-pHMR-1 is disordered. Thus, as in the mammalian case, phosphorylation stabilizes an extensive set of electrostatic and hydrophobic packing interactions that accounts for the large increase in affinity.

Although the backbone at residues 1211 and 1212 is positioned differently in conformations A and B (Figure 4A), the phosphate group of pS1212 is in almost the same position relative to HMP-2 and interacts with Tyr267, Arg271, Arg274, and Arg306 of HMP-2 (Figure 4B). Moreover, Ser1212 is the only phosphorylated residue that can be superimposed with the corresponding phospho-Ser (Ser686) among three visible phosphoserines (Ser684, Ser686, and Ser692) seen in the complex of phosphorylated E_{cyto} and β-catenin (Figure 4C).

To assess the contributions of S1212 and the other phosphosites to the affinity of HMR-1 for HMP-2, we produced and purified two different HMR-1 cytoplasmic tail mutants, S1212A and T1215A, and phosphorylated them in vitro with CKI. As expected for the consensus CKI sites processively phosphorylated starting at S1212 (Figure 2), mass spectrometry confirmed that S1212A was not phosphorylated in region IV, whereas T1215A retained phosphorylation at S1212 but lacked phosphorylation at S1218 and S1221 (data not shown). ITC measurements showed that HMP-$2_{54\text{-arm}}$ bound to HMR-1(S1212A)$_{cyto80}$ with essentially the same affinity as wild-type, non-pHMR-1_{cyto80}, whereas it bound strongly to pHMR-1(T1215A)$_{cyto80}$ with K_D = 26 nM, eight times weaker than that of the wild-type pHMR-1_{cyto80} (Table S2; Figure S2). Non-pHMR-1(T1215A)$_{cyto80}$ bound with K_D = 610 nM, 24 times weaker than the phosphorylated protein (Table S2; Figure S2). Like HMR-1(S1212A), there was no significant difference in affinity of HMP-2 for the non-pHMR-1(T1215A) versus wild-type HMR-1 (Table S2; Figure S2).

HMR-1 S1212 and S1218 are equivalent to two of the three residues recently identified as bearing the majority of vertebrate E-cadherin phosphorylation (Ser686 and Ser693, numbered from the mature sequence) (McEwen et al., 2014); the third phosphosite in the vertebrate cadherin, Ser692, is equivalent to HMR-1 E1217, a potential phosphomimetic. It is not known which of these phosphorylated residues contribute to the enhanced adhesion observed by McEwen et al. (2014). In the crystal structure of phosphorylated E-cadherin bound to β-catenin, pSer692 interacts extensively with β-catenin, whereas HMR-1 E1217 forms no contacts with HMP-2. Ser693 was not phosphorylated in the study of Huber and Weis (2001), and the equivalent HMR-1 pS1218 does not form direct contacts with HMP-2.

Collectively, the thermodynamic and structural data indicate that phosphorylation of the conserved S1212 contributes the majority of the affinity enhancement when the HMR-1 tail is phosphorylated by CK1, serving as a critical anchor point for the binding of region IV to HMP-2, enabling the large enhancement in affinity relative to the unphosphorylated HMR-1 (Figure 1A).

Phosphorylation of HMR-1 Ser1212 Is Essential for Cell Adhesion In Vivo

To test the functional significance of the HMR-1 pSer1212 interaction with HMP-2, in vivo rescue experiments were performed. The *hmr-1* allele *zu389* contains a nonsense mutation very early in the transcript and behaves as a genetic null, with homozygous mutant offspring dying embryonically with the Hammerhead phenotype. A full-length *hmr-1::gfp* transgene driven by the endogenous promoter (courtesy J. Nance, New York University) localizes to epidermal AJs and was able to rescue *hmr-1(zu389)* homozygotes to viability (Figures 5A and 5B). Site-directed mutagenesis was used to create a non-pHMR-1::GFP S1212A construct, which was then expressed in *hmr-1(zu389)*/+ unbalanced heterozygotes to assay for rescue. Although HMR-1(S1212A)::GFP localizes to junctions and is expressed at levels comparable to wild-type HMR-1 (Figures 5D and S3A), presumably due to having an intact extracellular adhesive domain, it fails to rescue *hmr-1(zu389)* homozygotes to viability. Most of these embryos die as Hammerhead (Figure 5C), indicative of full *hmr-1* loss of function.

HMR-1 pS1212 may also be necessary to prime additional phosphorylations at C-terminal CKI targets; as noted above, phosphorylation of these C-terminal sites contributes modestly to the affinity for HMP-2. In order to distinguish between the priming and direct HMP-2 interaction functions of HMR-1 S1212, we created an *hmr-1(T1215A, S1218A)::gfp*

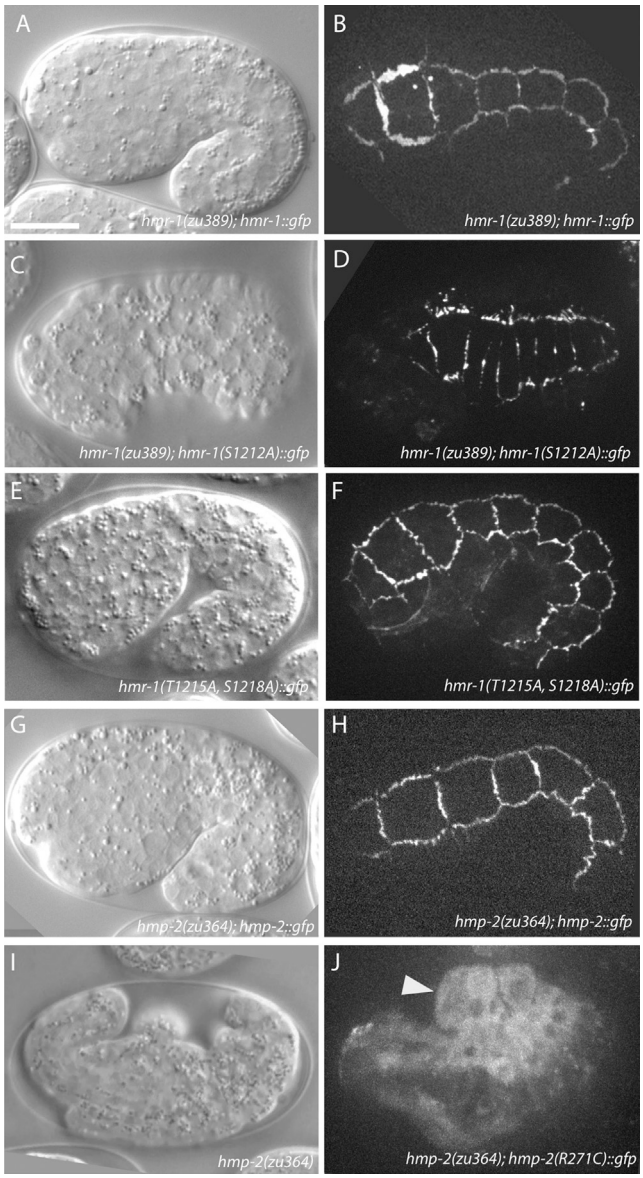

Figure 5. HMR-1 pS1212 Is Required for Interaction between HMP-2 and HMR-1

(A and B) Differential interference contrast (DIC) (A) and confocal (B) images of 1.5-fold elongating *hmr-1(zu389)* homozygotes rescued to viability by HMR-1::GFP. Lethality in offspring of *hmr-1(zu389); hmr-1::gfp* mothers is 85.2% (n = 209). Signal localizes to epidermal AJs similarly to HMR-1 immunostaining (not shown). Scale bar, 10 μm.

(C and D) The phospho null construct HMR-1(S1212A)::GFP localizes to junctions but is unable to rescue *hmr-1(zu389)* homozygotes to viability (C, DIC; D, confocal). Lethality in offspring of *hmr-1(zu389)/+; hmr-1(S1212A)::gfp* mothers is 27.4% (n = 1072). Cells in (D) appear compressed due to retraction of the hypodermis subsequent to failure of epiboly.

(E and F) HMR-1(T1215A, S1218A)::GFP localizes to junctions and rescues *hmr-1(zu389)* embryonic enclosure and elongation. The *hmr-1* transgene reduces embryonic lethality of *hmr-1(zu389)/+* offspring from 24.9% (n = 1101) to 16.9% (n = 1,055, three independent lines). Pictured is a representative offspring from a *hmr-1(zu389)/+; hmr-1(T1215A, S1218A)::gfp* mother (E, DIC; F, confocal).

(G and H) Wild-type HMP-2::GFP localizes to junctions (H) and rescues *hmp-2(zu364)* to viability (G).

(I) *hmp-2(zu364)* homozygotes fail to elongate and die with the Humpback phenotype. The *zu364* lesion was identified as a point mutation resulting in HMP-2 R271C.

(J) HMP-2(R271C)::GFP localizes exclusively to the cytoplasm, and embryos die with the Hmp phenotype, consistent with a model in which this residue is crucial for interacting with HMR-1 pS1212. Arrowhead indicates dorsal humps.

construct in which S1212 remains phosphorylatable, but the C-terminal phosphorylation cascade is blocked. HMR-1(T1215A, S1218A)::GFP localizes junctionally in wild-type and *hmr-1(zu389)/+* backgrounds and is able to partially rescue *hmr-1(zu389)* embryonic lethality (Figures 5E and 5F), but larval lethality precluded generation of a rescued *hmr-1(zu389)* homozygous line.

We also examined multiple conserved residues in HMP-2 that coordinate with pS1212 in HMR-1. Significantly, sequencing of a canonical strong *hmp-2* allele (*zu364)* revealed that one of the coordinating residues, Arg271, is mutated to a cysteine. A full-length *hmp-2::gfp* construct driven by 2 kb of endogenous promoter was expressed at epidermal adherens junctions and was able to rescue *hmp-2(zu364)* homozygotes to viability (Figures 5G and 5H). Re-creating the *zu364* allele in a *hmp-2::gfp* construct revealed that the protein is no longer recruited to adherens junctions and instead localizes diffusely to the cytoplasm (Figures 5I and 5J). As expected from its location on the exterior surface of the protein, this mutation does not alter protein folding or stability, as the recombinant protein could be prepared as a stable protein and was expressed at similar levels in animals (Figure S3B). ITC measurements revealed that HMP-2 R271C bound to pHMR-1 and HMR-1 with affinities that were the same as wild-type HMP-2 binding to non-pHMR-1, as expected for ablating the interaction of the R271 side chain with the phosphorylated S1212 (Table S2). Mutation of the other HMP-2 arginines in region IV to glutamic acids is predicted to ablate their ability to electrostatically bind HMR-1 pS1212. Consistent with this prediction, HMP-2::GFP R274E, R306E fails to rescue *hmp-2(zu364)* and localizes cytoplasmically, similarly to the R271C construct (data not shown).

Phosphorylation of HMP-2 Y599 May Regulate Junction Formation

Previous in vitro work has shown that Src phosphorylation of vertebrate β-catenin at Tyr654 in arm repeat 12 reduces its affinity for E-cadherin (Roura et al., 1999), and dephosphorylation of this residue is maintained in cell culture by the phosphatase PTP1B (Xu et al., 2004). The crystal structure of mouse β-catenin bound to E-cadherin revealed that Tyr654 forms a hydrogen bond with Asp665 of E-cadherin, so phosphorylation would disrupt this interaction (Huber and Weis, 2001). In two of the four crystallographically independent copies of the HMR-1/HMP-2 structure presented here, the equivalent tyrosine, Tyr599, forms a hydrogen bond with Glu1190 of HMR-1 (Figure 3C).

Although it is not known whether Tyr599 is phosphorylated in vivo, these data led us to examine the potential effect of this modification. We created phosphomimetic and phospho null mutations at amino acid 599 in *hmp-2::gfp*. Surprisingly, both

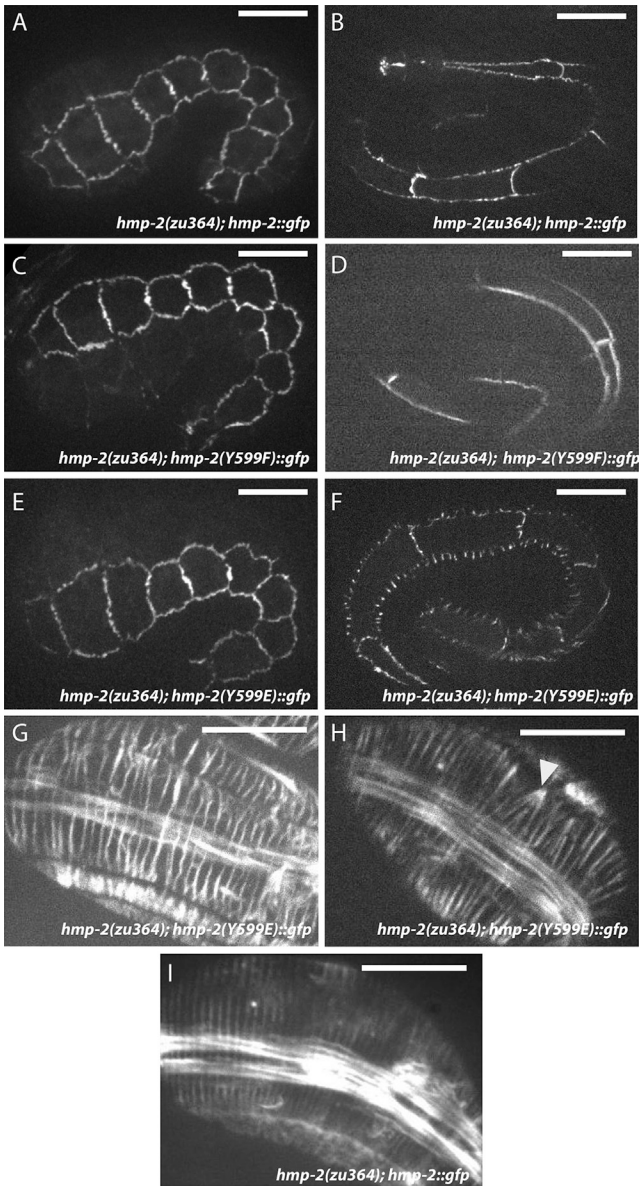

Figure 6. HMP-2 Y599E Localizes Aberrantly and Produces Mild CFB Defects

(A and B) Wild-type HMP-2::GFP signal is well established by early elongation (A) and is maintained at junctions through late elongation (B). Rescued *zu364* homozygotes display 53.9% lethality (n = 178), approximately commensurate with the transmission rate of the extrachromosomal array carrying the transgene. Scale bar, 10 μm.

(C and D) HMP-2(Y599F)::GFP rescues *hmp-2(zu364)* homozygotes and localizes to epidermal AJs identically to wild-type HMP-2::GFP both in early (C) and late (D) elongation. Rescued *zu364* homozygotes display 50.2% lethality (n = 305).

(E and F) HMP-2::GFP Y599E rescues *hmp-2(zu364)*. Signal initially localizes to AJs (E), but it becomes punctate during late elongation, and fluorescent excursions form orthogonally to junctions between lateral (seam) cells and their dorsal and ventral neighbors (F). Rescued *zu364* homozygotes display 45.9% lethality (n = 283).

(G–I) CFBs visualized by phalloidin staining in *hmp-2(zu364)* homozygotes rescued by wild-type (I) or Y599E (G and H) HMP-2::GFP constructs. Wild-type HMP-2::GFP embryos display evenly distributed radial F-actin bundles (I). CFBs in Y599E embryos become irregularly spaced (G and H), and occasionally multiple bundles aggregate to a single locus on the junction (H, arrowhead). Scale bar, 10 μm.

Y599E and Y599F constructs were able to rescue *hmp-2(zu364)* to a similar extent (45.9%, n = 283 and 50.2%, n = 305, respectively). However, although HMP-2::GFP Y599E initially localizes to AJs similarly to wild-type HMP-2::GFP (Figures 6A, 6E, and S3C), the junctional distribution becomes punctate during late elongation, and fluorescent signal forms excursions orthogonal to the junctions between lateral seam cells and their dorsal and ventral neighbors (Figure 6F).

Morphological defects observed in cadherin-catenin mutants often result from aberrant circumferential F-actin filament (CFB) organization in *C. elegans* embryos (Costa et al., 1998; Cox-Paulson et al., 2012; Maiden et al., 2013), as embryonic elongation is driven in large part by radially directed actomyosin-mediated tension transmitted to AJs via CFBs (Costa et al., 1998; Piekny et al., 2003). Phalloidin staining of *hmp-2(zu364)*; *hmp-2::gfp* Y599E embryos revealed modest defects in CFB organization, including wavy, irregularly spaced filaments, which could indicate a lack of maintenance of tension (Figures 6D and 6E), as well as occasional co-termination of multiple CFBs at a single point along the junction (Figure 6H). Surprisingly, HMP-2 Y599E and HMR-1 appear to colocalize in the excursions (Figure S4). This result suggests that loss of affinity between HMR-1 and HMP-2 leads to loss of resistance to lateral tension at junctions without complete abrogation of their interaction.

To understand the molecular mechanism of the Y599E phenotype, Glu was modeled at the position of Tyr599. The side chain of Glu can be accommodated in the interface with HMR-1 without steric collision or charge repulsion. However, Glu cannot form the extensive hydrophobic contacts with Ile1186 and Leu1189 of HMR-1, which could decrease HMP-2 affinity for HMR-1. Conversely, retention of these contacts may also explain the lack of obvious effects of the Y599F mutation. Furthermore, modeling suggests that phosphorylation at Tyr599 cannot be accommodated, as the phosphate group would be too close to the backbone carbonyl group of HMR-1 Leu1189 and the side chain of Glu1190. Thus, phosphorylation may reduce the interaction with region II of HMR-1.

Comparison with the SYS-1/POP-1 Complex

Previous yeast two-hybrid analyses suggested that HMR-1 cannot bind the other β-catenin paralogs in *C. elegans*, i.e., BAR-1, WRM-1, and SYS-1 (Kidd, 2005; Korswagen et al., 2000). Among the other β-catenin paralogs in *C. elegans*, only the structure of SYS-1 bound to POP-1, the *C. elegans* TCF homolog, is available (Liu et al., 2008). Comparison with the structure of the HMR-1/HMP-2 complex provides insight into why HMR-1 does not bind to these other β-catenin paralogs. Even though a POP-1 construct spanning residues 1–200 was present in the crystals of Liu et al. (2008), only residues 7–14 were visible. The polypeptide backbone of POP-1 residues 8–14 aligns well to pHMR-1_{cyto80} region III, residues 1199–1205, when arm repeats 7–9 of HMP-2 and SYS-1 are superimposed (Figure 7A). The critical salt bridge made by Asp8 of POP-1

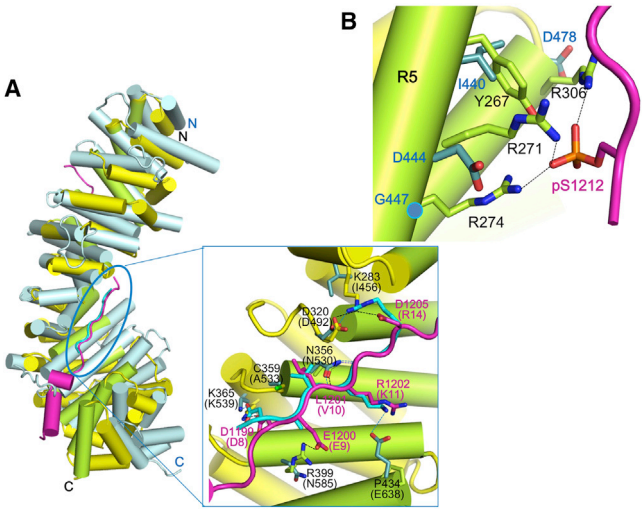

Figure 7. Structural Comparison of HMP-2/pHMR-1$_{cyto80}$ Complex with SYS-1/POP-1 Complex Suggests Why Only HMP-2 Can Bind pHMR-1

(A) Superposition of SYS-1/POP-1 (PDB ID: 3C2G) into HMP-2/pHMR-1$_{cyto80}$ complex. SYS-1 and POP-1 are colored light blue and cyan, respectively. Repeats 7–9 of SYS-1 and POP-1 are aligned to the corresponding regions of HMP-2 and pHMR-1. POP-1 (amino acids 8–14) aligns well with pHMR-1 region III, as shown in the close-up (boxed) view. SYS-1 and POP-1 residue numbers are in parentheses, and only those SYS-1 side chains that interact with POP-1 interaction are shown. The side chain of Glu9 of POP-1 was not modeled in the original structure. Hydrogen bonds in HMP-2/pHMR-1$_{cyto80}$ and SYS-1/POP-1 complexes are shown as black and blue dotted lines, respectively.

(B) Repeats 5 and 6 of SYS-1 are aligned to the corresponding region of HMP-2. The three arginine residues of HMP-2 that interact with pS1212 are not conserved in SYS-1.

and Lys539 of SYS-1 is preserved in the HMP-2/pHMR-1 structure (HMR-1 Asp1199 – HMP-2 Lys365), as are hydrogen bonds between Asn530 of SYS-1 and the polypeptide backbone of POP-1 (Figure 7A). Key hydrophobic packing interactions mediated by the Dxθθxφx$_{2-7}$E motif are also present. Nonetheless, we found that purified POP-1 (1–45), which is known to be sufficient for the interaction with SYS-1 and BAR-1 (Liu et al., 2008), does not bind to purified HMP-2 (data not shown).

The lack of binding between POP-1 and HMP-2 can be rationalized by aligning POP-1 with pHMR-1$_{cyto80}$ bound to HMP-2. Most POP-1 residues are accommodated without clashes with HMP-2. However, Arg14 is close to the side chain of Lys283 of HMP-2, which corresponds to Ile456 in SYS-1 (Figure 7A). POP-1 Arg14 forms a salt bridge with Asp492 of SYS-1, but in the HMP-2$_{arm}$/pHMR-1$_{cyto80}$ structure, Asp320 of HMP-2, which is equivalent to Asp492 of SYS-1, makes an intramolecular salt bridge with Lys283 and intermolecular interaction with Asp1205 of HMR-1 (Figure 3D). Although a different rotamer of Arg14 might avoid clashes, it would not be able to contribute to the interaction. Moreover, POP-1 Lys11 forms a salt bridge with SYS-1 Glu638, but this glutamate is replaced with Pro434 in HMP-2.

Although modeling suggests that HMR-1 regions II and III might be able to interact with SYS-1, the requirement for phosphorylation of region IV indicates that SYS-1 cannot bind to HMR-1 (pHMR-1). The HMP-2 residues that interact with the phosphate group of pSer1212, including Arg271, Arg274, and Arg306, are replaced with Asp444, Gly447, and Asp478 in SYS-1, which would prevent binding to the phosphorylated region IV (Figure 7B) by acting similarly to the charge reversal mutations in HMR-1 described above. Moreover, whereas HMP-2 Asn218 and Lys220 present on helix 3 of arm repeat 4 form hydrogen bonds with the polypeptide backbone of pHMR-1, this helix is shorter in SYS-1, and there are no residues in the same position as Asn218 and Lys220.

DISCUSSION

In this study, detailed biochemical and structural analysis of the interaction between HMR-1 and HMP-2, as well as comparison to mammalian E-cadherin and β-catenin, revealed conserved cadherin-catenin regulatory mechanisms that could be examined in a genetically tractable organism. Crucial among the interaction motifs we identified was HMR-1 S1212, homologous to murine E-cadherin S686, which functions as part of a phosphorylation switch for HMR-1/HMP-2 binding. While this work was in progress, a phosphoproteomics analysis of *C. elegans* embryos revealed that HMR-1 S1212 is in fact phosphorylated in vivo (A. Audhya, personal communication). Our results thus provide direct in vivo demonstration of how phosphorylation regulates cell-cell adhesion during tissue development.

HMR-1 S1212 is the first in a series of four consensus CKI sites that, when phosphorylated, increase affinity for HMP-2 120-fold in vitro (Figure 1; Table S2). This is consistent with previous in vitro studies of vertebrate homologs, in which phosphorylation of E-cadherin increased affinity for β-catenin by up to 800-fold (Choi et al., 2006). Vertebrate E-cadherin/β-catenin binding not only enables linkage between the cadherin-catenin complex and the actin cytoskeleton, but also imposes structure on the E-cadherin cytoplasmic tail. This structure renders the conserved ubiquitination and proteasomal degradation motif L-S-S-L within the PEST sequence of E-cadherin's cytoplasmic tail inaccessible (Huber et al., 2001; Huber and Weis, 2001). The purified HMR-1 cytoplasmic tail runs about three times larger than its predicted size on a gel filtration column, similar to the behavior of the unstructured E-cadherin cytoplasmic domain (Huber et al., 2001), consistent with its being an intrinsically unstructured protein. Thus, it is likely that the region around HMR-1 S1212 is disordered unless it is phosphorylated and bound to HMP-2. Whether this interaction protects a true PEST sequence in this region remains undetermined, although it is notable that HMR-1 contains the amino acid sequence L-E-S-I in a position homologous to the L-S-S-L motif in E-cadherin.

Phosphorylation of HMR-1 S1212 appears to be critical for stabilizing the HMR-1/HMP-2 association. In *C. elegans* embryos, non-pHMR-1 S1212A protein is unable to functionally substitute for wild-type HMR-1. That HMR-1(S1212A)::GFP and HMR-1(T1215A, S1218A)::GFP both target to AJs, but only the latter rescues *hmr-1(zu389)* embryonic lethality, suggests that mechanical uncoupling from HMP-2 due to the drastic loss in affinity is predominantly responsible for failure

to rescue. Nevertheless, the inability of *hmr-1(T1215A, S1218A)::gfp* to fully rescue the *hmr-1(zu389)* mutation suggests that although pS1212 is essential for strong binding to HMP-2, the C-terminal phosphorylations primed by pS1212, in particular T1215, are required for full HMR-1 function, consistent with its modest, but significant, contribution to binding of pHMR-1 to HMP-2 (Table S2). Although we cannot rule out a minor contribution due to proteasomal degradation of HMR-1, we did not detect appreciable quantitative reduction of HMR-1(S1212A)::GFP at junctions compared to wild-type HMR-1::GFP (Figure S3).

The HMR-1/HMP-2 co-crystal also identified the conserved HMP-2 residues R271, R274, and R306 as electrostatic partners with HMR-1 pS1212. Mutation of HMP-2 at these sites localizes the protein cytoplasmically and renders it unable to rescue *hmp-2(zu364)* embryos, confirming the importance of these residues in vivo. Further confirmation of this interaction comes from sequencing of the *hmp-2(zu364)* allele, which revealed that the mutation R271C is responsible for the genetic null phenotype and ablates the affinity enhancement provided by phosphorylation of the HMR-1 tail in vitro (Table S2). The importance of Arg271 to pHMR-1 binding is highlighted by its replacement by Asp444 in SYS-1, Gln324 of BAR-1, and Gln403 of WRM-1, none of which bind HMR-1. Analysis of HMP-2 also helps to explain phylogenetic diversification of β-catenins in *C. elegans*. Comparison of the HMR-1/HMP-2 and POP-1/SYS-1 structures, as well as the mutational data, indicates that SYS-1 lacks residues required for the high-affinity interaction with HMR-1. It may be that the arginine cluster needed for interaction of HMP-2 with pHMR-1 Ser1212 is incompatible with high-affinity binding to Wnt pathway partners.

HMR-1 lacks the C-terminal hydrophobic cap present in vertebrate cadherins, which contributes significantly to binding to β-catenin: even when not phosphorylated, E-cadherin binds to β-catenin with a K_D of 46 nM, and phosphorylation increases the affinity to 52 pM (Choi et al., 2006). It is interesting that pHMR-1 binds to HMP-2 with about the same affinity as non-phosphorylated E-cadherin binding to β-catenin and that phosphorylation also provides two to three orders of magnitude enhancement of affinity (Figure 1A). We speculate that the differences in absolute affinity reflect differences in the mechanical load experienced by the AJs in these two systems. Alternatively, it may be that *C. elegans* development requires a binary on/off switch for cell-cell adhesion that is provided by kinases and phosphatases acting on Ser1212.

HMP-2 Y599 is homologous to human and mouse β-catenin Y654, a phosphorylation site targeted by Src, FLT3, Abl, and PTP1B (Kajiguchi et al., 2012; Roura et al., 1999; Tamada et al., 2012; Xu et al., 2004). Previous in vitro work suggests that phosphorylation at β-catenin Y654 modestly decreases affinity for E-cadherin (Roura et al., 1999; van Veelen et al., 2011; Xu et al., 2004), suggesting a possible method of fine-tuning binding affinity. Our modeling indicates that phosphorylation of HMP-2 Y599 would not be accommodated in the region II interface (see above) but that HMP-2 Y599E could be accommodated in the HMP-2/HMR-1 complex, albeit with a loss of some packing interactions. In *D. melanogaster*, a putative phosphomimetic mutation at the homologous residue in Armadillo (Y667E) did not perturb binding to E-cadherin (Tamada et al., 2012); similarly, HMP-2 Y599E remains colocalized with HMR-1 in junctional excursions. These observations suggest that the Tyr→Glu mutation may not fully disrupt binding at the region II interface.

Interestingly, *Drosophila* Armadillo Y667E rescues β-catenin function during germband extension better than Y667F, in contrast to our work, in which the HMP-2 Y599E construct causes morphogenetic defects not seen with wild-type or Y599F rescue constructs. The different outcomes in the two systems may reflect differing biological requirements for junction dynamics. In the elongating *D. melanogaster* germband, AJs must be quickly remodeled in order to form multicellular rosettes that resolve into an elongated tissue. This could be facilitated through phosphorylation of β-catenin at Y667. In contrast, in the elongating *C. elegans* embryo, the organism as a whole is radially compressed via tensile force applied to CFBs, which are anchored at epidermal AJs. In this case, stabilizing β-catenin by dephosphorylation at Y599 could be advantageous for withstanding the force applied during embryonic elongation. Testing this idea awaits a means of unambiguously identifying individual posttranslational modifications of β-catenin in vivo at a subcellular level.

In summary, we have identified key cadherin/β-catenin interactions at atomic resolution and tested their functional significance in a living organism. Our data connect detailed atomic properties with specific developmental outcomes, providing structural insights into conserved binding interfaces through which cadherin-catenin binding affinity, and consequently intercellular adhesion, can be modulated according to the demands of a particular tissue or process. In addition, the functionally specialized β-catenin paralogs of *C. elegans* have enabled us to distinguish which features are critical for the association of E-cadherin to β-catenin and to discern adhesion-specific consequences of posttranslational modifications at these sites.

EXPERIMENTAL PROCEDURES

Construct Design and Protein Purification

Expression of full-length HMP-2 in *E. coli* did not yield soluble protein, whereas removing the first four amino acids produced a soluble protein. This construct lost another eight residues during purification, so the construct HMP-2_{13end} was produced for subsequent studies. Shorter constructs, based on the N-terminal boundary of the proteolytically defined arm domain of mouse β-catenin (Huber et al., 1997), start at residue 54. The C-terminal boundary of the arm domain was determined by the crystal structure of HMP-2_{54end}, and two constructs, HMP-2_{13arm} and HMP-2_{54arm}, comprising residues 13–621 and 54–621, respectively, were designed. The cytoplasmic domain of HMR-1, consisting of residues 1108–1223 and the minimal HMP-2 binding region, containing residues 1144–1223, were designed and labeled as HMR-1_{cyto} and HMR-1_{cyto80}, respectively.

Each protein was overexpressed with a tobacco etch virus (TEV) protease-cleavable GST tag at its N terminus. Proteins were purified by glutathione agarose affinity chromatography, and GST was removed by overnight treatment with TEV protease (20:1 substrate:TEV [w/w]) at 4°C. Each protein was subsequently purified by anion exchange (Mono Q; 20 mM Tris [pH 8.0], 0.5 mM EDTA, 2 mM DTT, run with a 100–350 mM NaCl gradient), followed by size exclusion chromatography on Superdex 200 (H buffer: 20 mM HEPES [pH 8.0], 150 mM NaCl, 1 mM DTT).

To generate pHMR-1, in vitro phosphorylation with CKI was performed as described previously (Kwiatkowski et al., 2010). In brief, phosphorylation was carried out for 12 hr at 30°C, and phosphorylated protein was separated

by Mono Q chromatography. Mass spectrometric analysis confirmed five phosphorylation sites in pHMR-1_{cyto} and four sites in pHMR-1_{cyto80}.

The HMP-2/pHMR-1 complex was purified by size exclusion chromatography after incubating the mixture of HMP-2_{54arm} and pHMR-1_{cyto80} in a 1:1.5 molar ratio for an hour at room temperature. Purified protein complex was concentrated to 20 mg ml^{-1} and used for crystallization.

Crystallization and Data Collection

Crystals of HMP-2_{54end} were grown by hanging drop vapor diffusion at 21°C by mixing protein solution with mother liquor of 1.3 M sodium formate and 50 mM HEPES (pH 7.5). The crystals were cryoprotected in perfluoropolyether oil (PFO). These crystals belong to space group C2, and there is one molecule in the asymmetric unit.

The complex of HMP-2_{54arm} and pHMR-1_{cyto80} was crystallized in two different forms. Needle-shaped crystals, space group $P2_1$ with three complexes in the asymmetric unit, were grown in 17% polyethylene glycol (PEG) 3350, 0.1 M Bis-Tris-propane (pH 8.0) and 0.2 M sodium sulfate. Crystals with plate-like morphology, space group $P4_3$ with one complex molecule in the asymmetric unit, were obtained with the same condition except that 0.2 M sodium iodide was used instead of sodium sulfate. In both cases, the crystals were cryoprotected in the same mother liquor except that the PEG3350 concentration was raised to 20%, and 20% glycerol was present. Diffraction data were measured at 100 K on beamline 11-1 at Stanford Synchrotron Radiation laboratory (SSRL) and processed with HKL2000 (Table S1).

Structure Determination and Refinement

The structure of HMP-2_{54end} was solved by molecular replacement (MR) with Phaser, using the mouse β-catenin arm domain structure as a search model (PDB ID: 1I7W). The structure was refined with PHENIX and Coot. The final refined model consists of HMP-2 residues 56–612.

The structure of the HMP-2/pHMR-1_{cyto80} complex was solved by MR using the refined structure of HMP-2_{54end} as a search model. Initial maps calculated using phases from the model of the MR solution showed extra density corresponding to HMR-1. Iterative cycles of manual rebuilding with Coot and refinement with Phenix were performed to produce the final model (Table S1). The final model in $P4_3$ contains HMP-2 residues 77–613 and HMR-1 residues 1145–1152 and 1179–1212. In the $P2_1$ crystal, copy A consists of HMP-2 residues 81–88 and 91–614 and HMR-1 residues 1145–1152 and 1179–1213; copy B comprises HMP-2 residues 78–613 and HMR-1 residues 1145–1152 and 1179–1213; and copy C comprises HMP-2 residues 82–107, 120–522, and 531–607 and HMR-1 residues 1182–1207 and 1211–1222.

ITC

ITC experiments were carried out in a VP-ITC calorimeter (Microcal, GE Healthcare) at 25°C. The cell contained 8–12 μM HMP-2 protein and 7–10 μl of 100–150 μM HMR-1 (non-phospho and phospho) was injected 20–36 times, following two initial 2-μl injections. Data were analyzed using Microcal Origin software package.

C. elegans Constructs and Strains

pJN455[$P_{hmr\text{-}1}$*::hmr-1::gfp*] (Achilleos et al., 2010) was mutagenized using circle PCR to generate pTDL51[$P_{hmr\text{-}1}$*::hmr-1(S1212A)::gfp*] and pTDL128 [$P_{hmr\text{-}1}$*::hmr-1(T1215A, S1218A)::gfp*]. Forward S1212A PCR primer: 5′-GCT GTC GTC ACG TTG GAG AGT ATC-3′. Reverse PCR primer: 5′-AAT ATT GTC CCG CTC ATC G-3′. Forward T1215A, S1218A primer: 5′-GCT ATC GAA AGT GCC CAA GG-3′. Reverse primer: 5′-CTC CAA CGC GAC GAC AGA AAT ATT-3′. Underlined bases indicate mutation sites.

2 kb of endogenous *hmp-2* promoter was amplified from genomic DNA and cloned into pPD95.75 to generate pTDL33, into which *hmp-2* cDNA yk1047c6 was cloned to generate pTDL34[$P_{hmp\text{-}2}$*::hmp-2::gfp*]. R271 and Y599 mutations were generated using circle PCR with the pTDL34 template.

The *hmr-1* null allele *zu389* was maintained as an unbalanced heterozygote. Presence of the *zu389* allele was determined by dead embryo counts and by restriction digest and gel electrophoresis of PCR amplicons from worm lysates. Hermaphrodites were allowed to lay embryos for 24 hr before being lysed as described previously (Williams et al., 1992). Forward primer flanking the *zu389* locus: 5′-TTT CAT GCT TTT TCC CCA AA-3′. Reverse flanking primer: 5′-CCA CAG CCT ACA ACC CTT TT-3′. PCR produces a 966-nt amplicon that is cleaved into 650- and 316-nt fragments by DdeI when the *zu389* mutation is present.

hmr-1(zu389)/+ I; jcEx198 was generated by injecting pTDL51 into N2 at a concentration of 2 ng/μl and crossing into *hmr-1(zu389)* heterozygotes. *hmr-1(zu389) I; jcEx208 and hmr-1(zu389)/+ I; jcEx247* were generated by injecting pJN455 and pTDL128, respectively, into *hmr-1(zu389)* heterozygotes.

For mutant allele sequencing, homozygous mutant *hmp-2(zu364)* embryos were identified, isolated, frozen, lysed, and sequenced as previously described (Kwiatkowski et al., 2010). All *hmp-2* transgenic lines were generated by injecting pTDL34 or one of its mutant derivatives at 20 ng/μl into *hmp-2(zu364)* heterozygotes.

Bristol N2 was used as the wild-type *C. elegans* strain. All worms were fed OP50 nematode growth media and maintained at 20°C (Brenner, 1974).

Phalloidin Staining

Embryos were collected by dissolving gravid adults in a solution of 250 mM KOH and 0.5% NaOCl for 5 min, and then they were washed twice with distilled deionized water and mounted on poly-L-lysine-coated ring slides. Embryos were fixed in a solution of 4% paraformaldehyde, 10 mM EGTA (pH 8), 25 mM HEPES (pH 6.8), 48 mM PIPES (pH 6.8), 2 mM $MgCl_2$, and 0.2% Triton X-100 for 20 min at room temperature in a humid chamber. Fixed embryos were washed twice with PBS for 5 min and then incubated with Texas red-conjugated phalloidin for 2 hr at room temperature in a humid chamber, protected from light. Slides were then washed twice with PBS for 5 min. Antifade reagent was added to each sample before coverslips were applied and sealed with nail polish.

Microscopy and Image Analysis

Rabbit HMR-1 and HMP-2 antibodies were used at 1 μg/ml. Staining was performed as described previously (Maiden et al., 2013). Mouse monoclonal GFP antibody was used at 0.2 μg/ml (Molecular Probes).

Microscopy of live embryos was performed using a Nikon Eclipse E600 microscope with a Yokogawa CSU10 spinning disk scanhead. Images were obtained using a Hamamatsu ORCA-ER charge-coupled device (CCD) camera and Micromanager software. Four-dimensional movies were processed and analyzed using ImageJ (Hardin, 2011). Images are Z-projections of three to four focal planes spaced 1.0 μm apart. Fluorescence recovery after photobleaching (FRAP) images were acquired with an Olympus FluoView FV1000 microscope.

Fluorescence quantitation was performed in ImageJ. Junctions were isolated by thresholding Z-projections of two focal planes to 99% and selected using the wand tool. Mean fluorescence per pixel for identical seam-dorsal and seam-ventral junctions were compared between embryos. To compare junctional HMP-2::GFP expression to cytoplasmic HMP-2(R271C)::GFP, 20 focal planes of each embryo were sum projected, and mean fluorescence per pixel was calculated for each embryo after subtraction of background signal.

ACCESSION NUMBERS

The PDB accession codes for the structures reported in this paper are 4R0Z (HMP-$2_{54\text{-}end}$), 4R10 (HMP-2/HMR-1, $P4_3$ crystal form), and 4R11(HMP-2/HMR-1, $P2_1$ crystal form).

SUPPLEMENTAL INFORMATION

Supplemental Information includes four figures and two tables and can be found with this article online at http://dx.doi.org/10.1016/j.devcel.2015.02.005.

AUTHOR CONTRIBUTIONS

H.-J.C., T.L., J.H., and W.I.W. conceived the experiments and wrote the paper. H.-J.C. performed the purification, biochemical and biophysical measurements, and crystallographic structure determination of HMP-2 and HMP2/HMR-1 complexes. T.L. performed cloning and site-directed mutagenesis of HMP-2 and HMR-1 constructs; made *hmp-2* and *hmr-1* transgenic

lines; and performed staining, microscopy, image analysis, and rescue assessment of mutants carrying *hmp-2* and *hmr-1* transgenes. A.M.L. prepared *hmp-2(zu364)* embryos for sequencing, made a *hmr-1:S1212A::gfp* transgenic line and related strains, and characterized *hmr-1(zu389)*/+; *hmr-1S1212A::gfp* embryos. I.B. purified HMP-2 and HMR-1 mutants and performed ITC measurements on their interactions.

ACKNOWLEDGMENTS

We thank Dr. Jon Audhya for sharing his unpublished mass spectrometry data on HMR-1 and Bethany Lucas for assistance with DNA microinjections. This work was supported by the Research Settlement Fund for the new faculty of SNU and Basic Science Research Program through the NRF funded by the Ministry of Education (NRF-2013R1A1A2061541) (H.-J.C.), NIH grants R21 HD072769 and R01 GM58038 (J.H.), and NIH grants R01 GM56169 and U01 GM09463 (W.I.W.). Portions of this work were performed at the Stanford Synchrotron Radiation Lightsource, supported by the U.S. Department of Energy and NIH.

Received: July 31, 2014
Revised: December 20, 2014
Accepted: February 5, 2015
Published: April 6, 2015

REFERENCES

Achilleos, A., Wehman, A.M., and Nance, J. (2010). PAR-3 mediates the initial clustering and apical localization of junction and polarity proteins during C. elegans intestinal epithelial cell polarization. Development *137*, 1833–1842.

Barker, N., Hurlstone, A., Musisi, H., Miles, A., Bienz, M., and Clevers, H. (2001). The chromatin remodelling factor Brg-1 interacts with beta-catenin to promote target gene activation. EMBO J. *20*, 4935–4943.

Bek, S., and Kemler, R. (2002). Protein kinase CKII regulates the interaction of β-catenin with α-catenin and its protein stability. J. Cell Sci. *115*, 4743–4753.

Benjamin, J.M., and Nelson, W.J. (2008). Bench to bedside and back again: molecular mechanisms of α-catenin function and roles in tumorigenesis. Semin. Cancer Biol. *18*, 53–64.

Brenner, S. (1974). The genetics of Caenorhabditis elegans. Genetics *77*, 71–94.

Choi, H.-J., Huber, A.H., and Weis, W.I. (2006). Thermodynamics of β-catenin-ligand interactions: the roles of the N- and C-terminal tails in modulating binding affinity. J. Biol. Chem. *281*, 1027–1038.

Choi, H.J., Gross, J.C., Pokutta, S., and Weis, W.I. (2009). Interactions of plakoglobin and β-catenin with desmosomal cadherins: basis of selective exclusion of α- and β-catenin from desmosomes. J. Biol. Chem. *284*, 31776–31788.

Costa, M., Raich, W., Agbunag, C., Leung, B., Hardin, J., and Priess, J.R. (1998). A putative catenin-cadherin system mediates morphogenesis of the *Caenorhabditis elegans* embryo. J. Cell Biol. *141*, 297–308.

Cox, E.A., and Hardin, J. (2004). Sticky worms: adhesion complexes in C. elegans. J. Cell Sci. *117*, 1885–1897.

Cox-Paulson, E.A., Walck-Shannon, E., Lynch, A.M., Yamashiro, S., Zaidel-Bar, R., Eno, C.C., Ono, S., and Hardin, J. (2012). Tropomodulin protects α-catenin-dependent junctional-actin networks under stress during epithelial morphogenesis. Curr. Biol. *22*, 1500–1505.

Finnemann, S., Mitrik, I., Hess, M., Otto, G., and Wedlich, D. (1997). Uncoupling of XB/U-cadherin-catenin complex formation from its function in cell-cell adhesion. J. Biol. Chem. *272*, 11856–11862.

Hardin, J. (2011). Imaging embryonic morphogenesis in *C. elegans*. In Methods In Cell Biology, *Vol. 106*, J.H. Rothman and A. Singson, eds. (Academic Press), pp. 377–412.

Hecht, A., Litterst, C.M., Huber, O., and Kemler, R. (1999). Functional characterization of multiple transactivating elements in beta-catenin, some of which interact with the TATA-binding protein in vitro. J. Biol. Chem. *274*, 18017–18025.

Hecht, A., Vleminckx, K., Stemmler, M.P., van Roy, F., and Kemler, R. (2000). The p300/CBP acetyltransferases function as transcriptional coactivators of beta-catenin in vertebrates. EMBO J. *19*, 1839–1850.

Huber, A.H., and Weis, W.I. (2001). The structure of the β-catenin/E-cadherin complex and the molecular basis of diverse ligand recognition by β-catenin. Cell *105*, 391–402.

Huber, A.H., Nelson, W.J., and Weis, W.I. (1997). Three-dimensional structure of the armadillo repeat region of β-catenin. Cell *90*, 871–882.

Huber, A.H., Stewart, D.B., Laurents, D.V., Nelson, W.J., and Weis, W.I. (2001). The cadherin cytoplasmic domain is unstructured in the absence of β-catenin. A possible mechanism for regulating cadherin turnover. J. Biol. Chem. *276*, 12301–12309.

Kajiguchi, T., Katsumi, A., Tanizaki, R., Kiyoi, H., and Naoe, T. (2012). Y654 of β-catenin is essential for FLT3/ITD-related tyrosine phosphorylation and nuclear localization of β-catenin. Eur. J. Haematol. *88*, 314–320.

Kidd, A.R. (2005). SYS-1, a β-catenin identified by functional criteria is required for asymmetric cell divisions in the nematode *Caenorhabditis elegans*. PhD thesis. (Madison: University of Wisconsin).

Korswagen, H.C., Herman, M.A., and Clevers, H.C. (2000). Distinct β-catenins mediate adhesion and signalling functions in *C. elegans*. Nature *406*, 527–532.

Kwiatkowski, A.V., Maiden, S.L., Pokutta, S., Choi, H.J., Benjamin, J.M., Lynch, A.M., Nelson, W.J., Weis, W.I., and Hardin, J. (2010). In vitro and in vivo reconstitution of the cadherin-catenin-actin complex from Caenorhabditis elegans. Proc. Natl. Acad. Sci. USA *107*, 14591–14596.

Lickert, H., Bauer, A., Kemler, R., and Stappert, J. (2000). Casein kinase II phosphorylation of E-cadherin increases E-cadherin/β-catenin interaction and strengthens cell-cell adhesion. J. Biol. Chem. *275*, 5090–5095.

Liu, J., Phillips, B.T., Amaya, M.F., Kimble, J., and Xu, W. (2008). The *C. elegans* SYS-1 protein is a bona fide β-catenin. Dev. Cell *14*, 751–761.

Maiden, S.L., Harrison, N., Keegan, J., Cain, B., Lynch, A.M., Pettitt, J., and Hardin, J. (2013). Specific conserved C-terminal amino acids of Caenorhabditis elegans HMP-1/α-catenin modulate F-actin binding independently of vinculin. J. Biol. Chem. *288*, 5694–5706.

McEwen, A.E., Maher, M.T., Mo, R., and Gottardi, C.J. (2014). E-cadherin phosphorylation occurs during its biosynthesis to promote its cell surface stability and adhesion. Mol. Biol. Cell *25*, 2365–2374.

Miyagishi, M., Fujii, R., Hatta, M., Yoshida, E., Araya, N., Nagafuchi, A., Ishihara, S., Nakajima, T., and Fukamizu, A. (2000). Regulation of Lef-mediated transcription and p53-dependent pathway by associating beta-catenin with CBP/p300. J. Biol. Chem. *275*, 35170–35175.

Piekny, A.J., Johnson, J.-L.F., Cham, G.D., and Mains, P.E. (2003). The Caenorhabditis elegans nonmuscle myosin genes nmy-1 and nmy-2 function as redundant components of the let-502/Rho-binding kinase and mel-11/myosin phosphatase pathway during embryonic morphogenesis. Development *130*, 5695–5704.

Pokutta, S., and Weis, W.I. (2007). Structure and mechanism of cadherins and catenins in cell-cell contacts. Annu. Rev. Cell Dev. Biol. *23*, 237–261.

Roura, S., Miravet, S., Piedra, J., García de Herreros, A., and Duñach, M. (1999). Regulation of E-cadherin/Catenin association by tyrosine phosphorylation. J. Biol. Chem. *274*, 36734–36740.

Stamos, J.L., and Weis, W.I. (2013). The β-catenin destruction complex. Cold Spring Harb. Perspect. Biol. *5*, a007898.

Stappert, J., and Kemler, R. (1994). A short core region of E-cadherin is essential for catenin binding and is highly phosphorylated. Cell Adhes. Commun. *2*, 319–327.

Takemaru, K.I., and Moon, R.T. (2000). The transcriptional coactivator CBP interacts with beta-catenin to activate gene expression. J. Cell Biol. *149*, 249–254.

Tamada, M., Farrell, D.L., and Zallen, J.A. (2012). Abl regulates planar polarized junctional dynamics through β-catenin tyrosine phosphorylation. Dev. Cell *22*, 309–319.

Tutter, A.V., Fryer, C.J., and Jones, K.A. (2001). Chromatin-specific regulation of LEF-1-β-catenin transcription activation and inhibition in vitro. Genes Dev. *15*, 3342–3354.

van Roy, F. (2014). Beyond E-cadherin: roles of other cadherin superfamily members in cancer. Nat. Rev. Cancer *14*, 121–134.

van Veelen, W., Le, N.H., Helvensteijn, W., Blonden, L., Theeuwes, M., Bakker, E.R.M., Franken, P.F., van Gurp, L., Meijlink, F., van der Valk, M.A., et al. (2011). β-catenin tyrosine 654 phosphorylation increases Wnt signalling and intestinal tumorigenesis. Gut *60*, 1204–1212.

Williams, B.D., Schrank, B., Huynh, C., Shownkeen, R., and Waterston, R.H. (1992). A genetic mapping system in Caenorhabditis elegans based on polymorphic sequence-tagged sites. Genetics *131*, 609–624.

Xing, Y., Takemaru, K., Liu, J., Berndt, J.D., Zheng, J.J., Moon, R.T., and Xu, W. (2008). Crystal structure of a full-length β-catenin. Structure *16*, 478–487.

Xu, G., Craig, A.W.B., Greer, P., Miller, M., Anastasiadis, P.Z., Lilien, J., and Balsamo, J. (2004). Continuous association of cadherin with β-catenin requires the non-receptor tyrosine-kinase Fer. J. Cell Sci. *117*, 3207–3219.

Developmental Cell

Supplemental Information

A Conserved Phosphorylation Switch Controls the Interaction between Cadherin and β-Catenin In Vitro and In Vivo

Hee-Jung Choi, Timothy Loveless, Allison M. Lynch, Injin Bang, Jeff Hardin, and William I. Weis

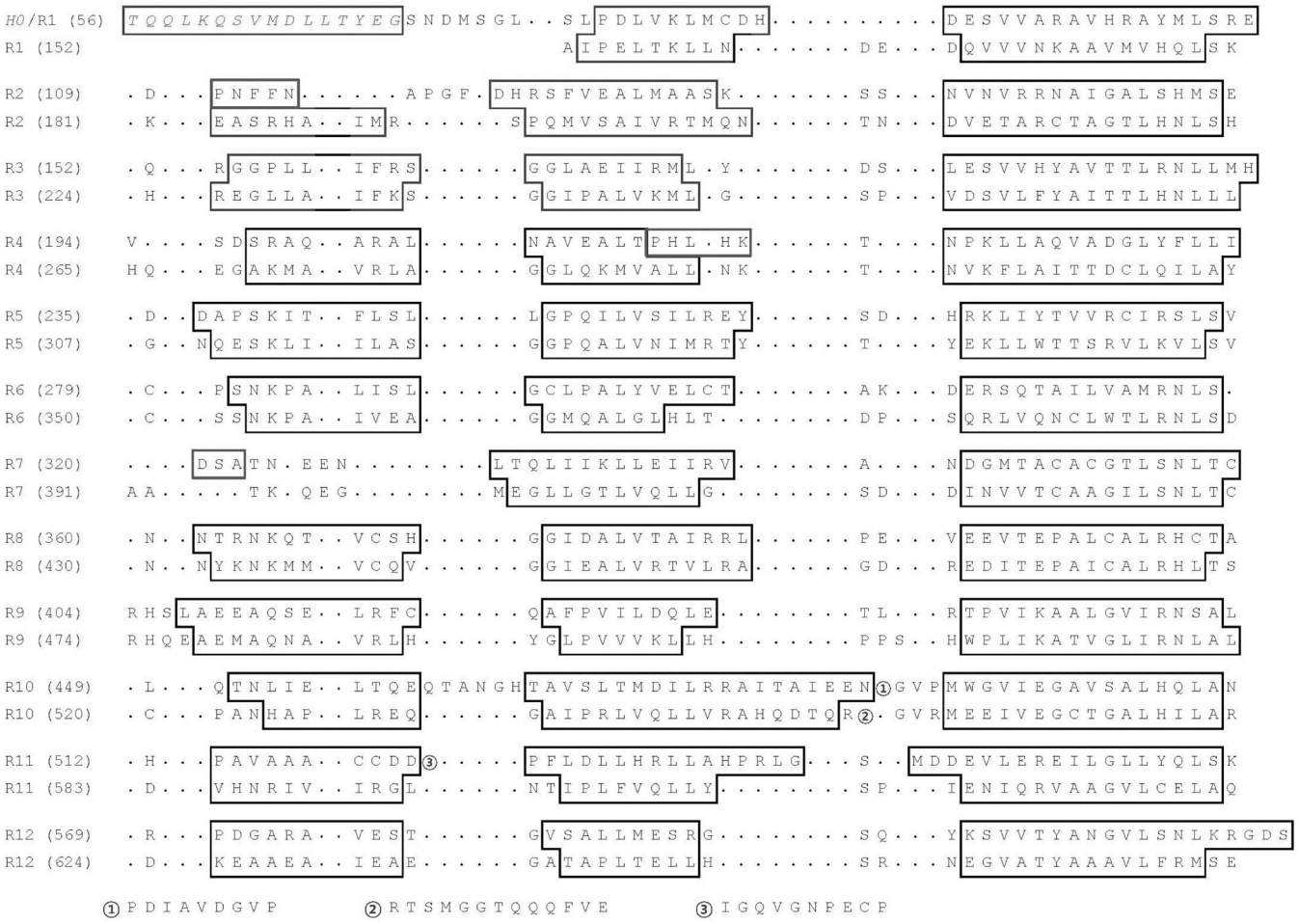

Figure S1, related to Figure 1. Alignment of the armadillo domains of *C. elegans* HMP-2 and *M. musculus* β-catenin. The boxed regions correspond to α helices H1, H2 and H3 left to right, as observed in the respective crystal structures. Italicized residues are present in the crystallized construct but not visible. The circled numbers correspond to loop sequences inserted at those positions and shown at the bottom.

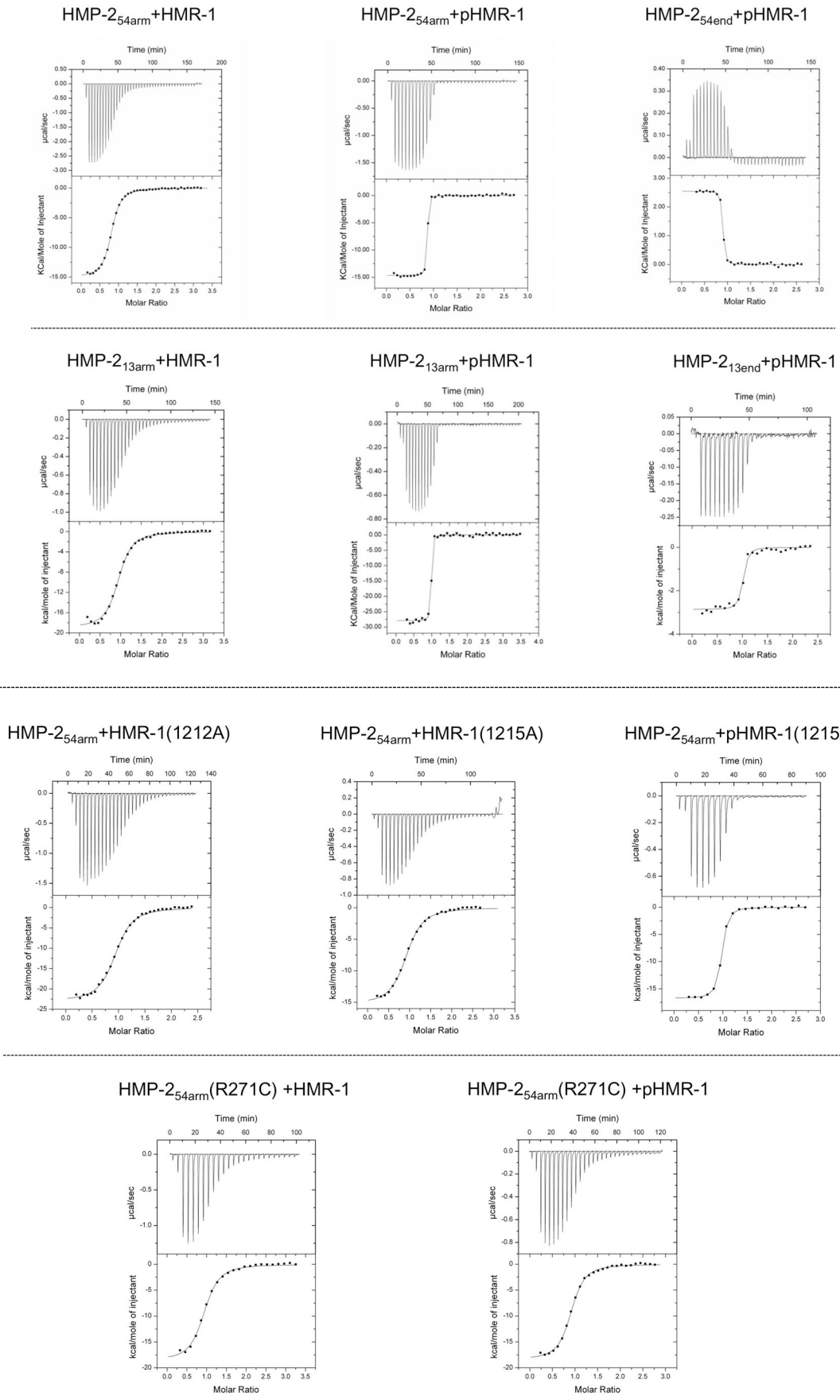

Figure S2, related to Figure 1 and Table S2. Isothermal titration calorimetry traces for the indicated binding reactions.

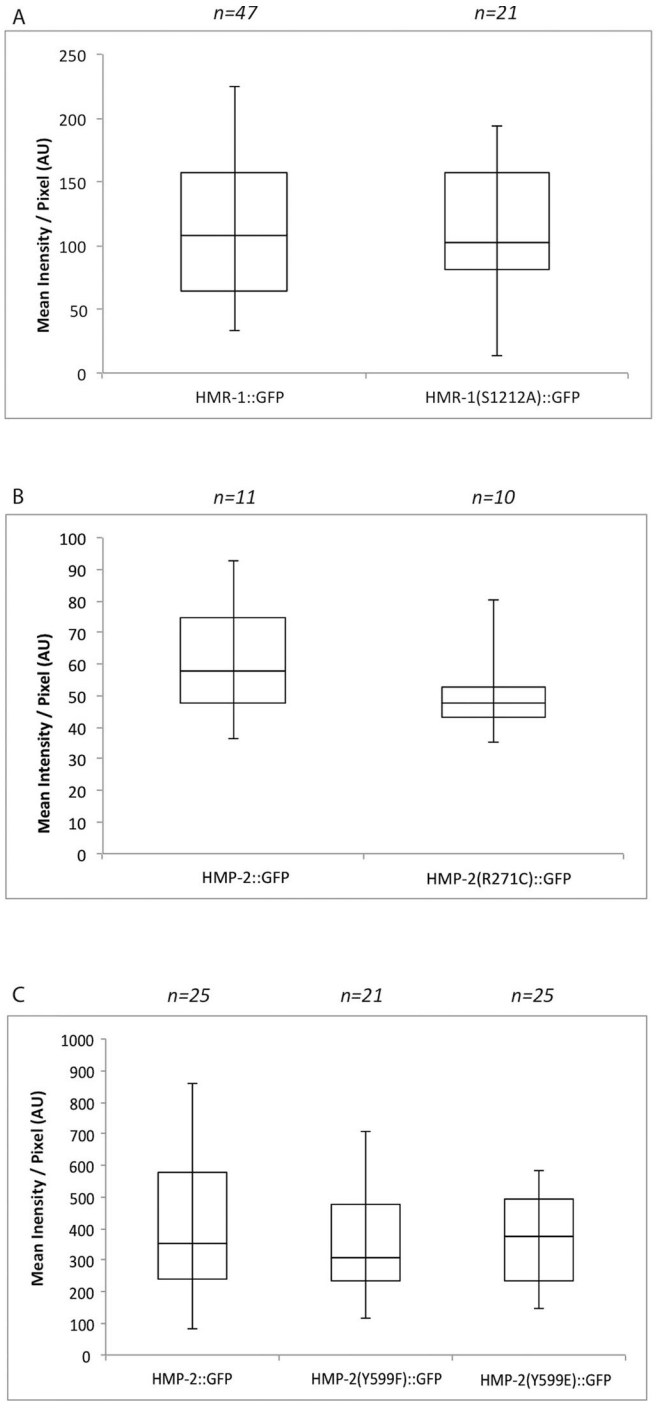

Figure S3, related to Figure 5 and 6. (A) Quantitation of HMR-1::GFP vs. HMR-1(S1212A)::GFP found no significant difference in expression levels ($p = 0.7100$, two-tailed t-test, n = number of individual junctions measured). Z-projections of 2 focal planes were measured for each junction. (B) Quantitation of HMP-2::GFP vs. HMP-2(R271C)::GFP found no significant difference in expression levels ($p = 0.6549$, two-tailed t-test, n = number of embryos scored). 20 focal planes were sum projected for each embryo. Mean fluorescence of each embryo was corrected for mean fluorescence of a background ROI in each image. (C) Quantitation of HMP-2::GFP vs. HMP-2(Y599F)::GFP vs. HMP-2(Y599E)::GFP found no significant difference in expression levels ($p = 0.4588$, one way ANOVA, n = number of individual junctions measured). Z-projections of 2 focal planes were measured for each junction.

AU = arbitrary units.

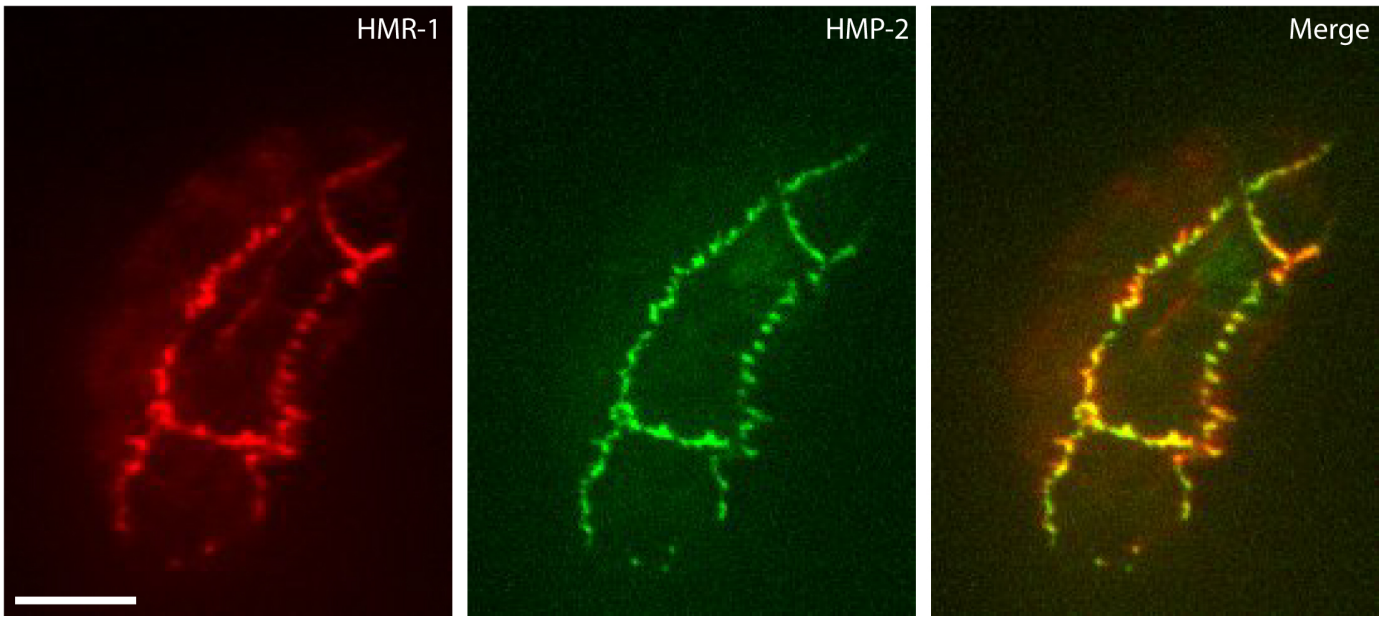

Figure S4, related to Figure 6. Co-immunostaining of a 4-fold *hmp-2(zu364); hmp-2(Y599E)::gfp* embryo with anti-HMR-1 antibody (red) and anti-GFP antibody (green). HMR-1 signal is discontinuous along cell-cell junctions and colocalizes with HMP-2(Y599E) excursions. Scale bar is 10 μm.

Table S1, related to Figures 1, 3, 4 and 7. Crystallographic statistics.

Data collection	*HMP-2$_{54end}$*	*HMP-2$_{54arm}$+phosphoHMR-1$_{cyto80}$*	
wavelength (Å)	1.0332	0.97945	0.97945
Space group	C2	$P2_1$	$P4_3$
Unit cell parameters			
a(Å)	165.2	85.1	84.7
b(Å)	39.0	157.7	84.7
c(Å)	101.1	84.8	137.0
β(°)	116.7	94.2	90.0
Resolution (Å) (last shell)	50-2.0 (2.07-2.00)	50-2.8 (2.9-2.8)	50-2.3 (2.38-2.3)
Unique reflections	36,385 (3154)	54,788 (5272)	42,695 (4189)
Completeness (%)	93.0 (82.7)	99.3 (95.9)	99.6 (99.3)
Multiplicity	4.9 (4.4)	3.6 (3.4)	3.9 (3.9)
$\langle I/\sigma(I)\rangle$	19.7 (5.6)	11.8 (2.1)	17.9 (4.5)
R_{merge}[a]	0.038 (0.22)	0.048 (0.54)	0.03 (0.36)
$CC_{1/2}$	0.999 (0.978)	0.997 (0.810)	0.998 (0.873)
Refinement			
No. reflections working set / test set	36,351 / 2783	54,463 / 4242	42,679 / 3288
R_{cryst} / R_{free}[b]	0.19 / 0.23	0.20 / 0.25	0.17 / 0.20
bond length rmsd from ideal (Å)	0.003	0.003	0.003
bond angle rmsd from ideal (°)	0.75	0.74	0.72
Ramachandran analysis[c]			
% favored regions	95.8	94.3	95.8
% allowed regions	4.2	5.7	4.2
% outliers	0.0	0.0	0.0

rmsd, root-mean square deviation.

[a]$R_{merge}=\Sigma_h\Sigma_l|I_i h<Ih>|\Sigma_h\Sigma_i(h)$, where $I_i(h)$ is the i^{th} measurement of reflection h, and $\langle I(h)\rangle$ is the weighted mean of all measurements of h.

[b]$R = \Sigma_h|F_{obs}(h)| - |F_{calc}(h)| \,| / \Sigma_h|F_{obs}(h)|$. $R_{cryst}$and R_{free}were calculated using the working and test reflection sets, respectively.

[c]As defined in MolProbity

Table S2, related to Figures 1 and S2. ITC measurements of HMP-2 binding to phosphorylated and non-phosphorylated HMR-1. Representative traces are shown in Figure S2. ND, no detectable binding.

Proteins		K_D (nM)	ΔH (kcal mol^{-1})	TΔS (kcal mol^{-1})	ΔG (kcal mol^{-1})
HMP-2_{13end}	HMR-1_{cyto80}	ND	-	-	-
HMP-2_{13end}	pHMR-1_{cyto80}	51.3	-2.9	7.1	-9.9
HMP-2_{54end}	HMR-1_{cyto80}	ND	-	-	-
HMP-2_{54end}	pHMR-1_{cyto80}	23.0	2.5	13.0	-10.5
HMP-2_{13arm}	HMR-1_{cyto80}	382	-19.0	-10.3	-8.7
HMP-2_{13arm}	pHMR-1_{cyto80}	7.9	-18.6	-7.5	-11.1
HMP-2_{54arm}	HMR-1_{cyto80}	380	-19.2	-10.5	-8.7
HMP-2_{54arm}	pHMR-1_{cyto80}	3.1	-27.9	-16.3	-11.6
HMP-2_{54arm}	HMR-1_{cyto80} (S1212A)	518	-23.0	-14.4	-8.6
HMP-2_{54arm}	HMR-1_{cyto80} (T1215A)	610	-15.4	-6.9	-8.5
HMP-2_{54arm}	pHMR-1_{cyto80} (T1215A)	25.6	-16.7	-6.4	-10.3
HMP-2_{54arm} (R271C)	HMR-1_{cyto80}	435	-18.7	-10.0	-8.7
HMP-2_{54arm} (R271C)	pHMR-1_{cyto80}	249	-18.5	-9.4	-9.1